UC San Diego
Technical Reports

Title

A Practical Microcylinder Appearance Model for Cloth Rendering

Permalink

https://escholarship.org/uc/item/6v11p5b0

Authors

Sadhegi, Iman
Bisker, Oleg
De Deken, Joachim
et al.

Publication Date

2012-04-05

Peer reviewed

A Practical Microcylinder Appearance Model for Cloth Rendering

Iman Sadeghi   Oleg Bisker   Joachim De Deken   Henrik Wann Jensen
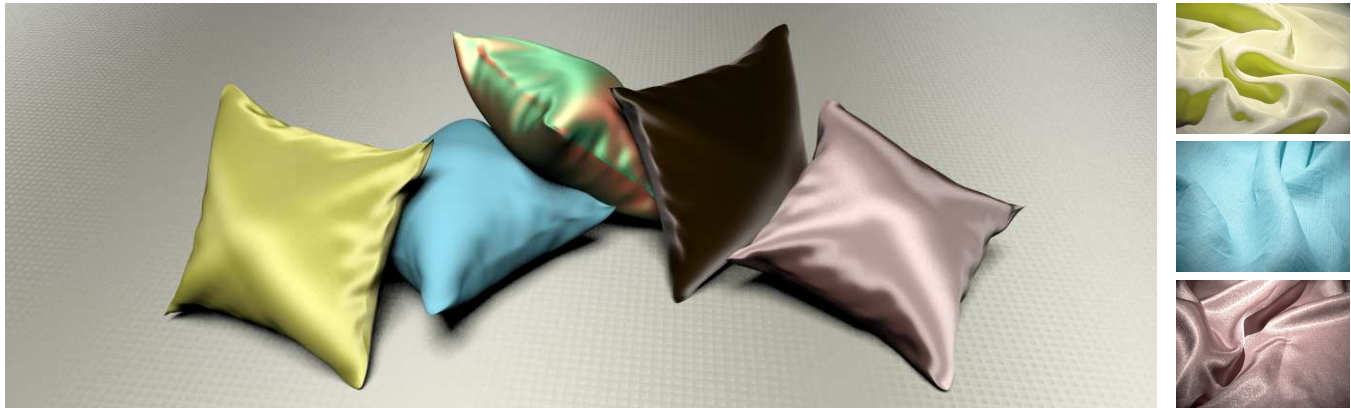
University of California, San Diego

Figure 1: *Image rendered using our microcylinder shading model with intuitive parameters for different fabric types. Left to right the fabrics are: Silk Crepe de Chine, Linen Plain, Silk Shot Fabric, Velvet, and Polyester Satin Charmeuse. (right) Reference photos for three of the fabrics rendered.*

Abstract

This paper introduces a simple shading model for cloth. The model can simulate both the anisotropic highlights on cloth as well as the complex color shifts seen in cloth made of different colored threads. Our model is based on extensive Bidirectional Reflectance Distribution Function (BRDF) measurements of several cloth samples. We have also measured the scattering profile of several different individual cloth threads. Based on these measurements we have derived a simple model capable of predicting the light scattered by different threads. We model cloth as a collection of threads in a weave pattern which provides information about the coverage of the different thread types as well as their tangent directions. Our model also accounts for shadowing and masking by the threads. We validate our model by comparing predicted and measured values and we show how we can use the model to recover parameters for different cloth samples including silk, velvet, linen, and polyester with varying weaving patterns. We can also, model the appearance of novel physically plausible cloth fabrics. Finally, we demonstrate that our model can run in real-time on a GPU.

CR Categories: I.3.7 [Computer Graphics]: Three-Dimensional Graphics and Realism—Rendering;

Keywords: cloth, microcylinders, appearance modeling, weaving pattern, anisotropic BRDF

1 Introduction

Cloth is a complex material made of interwoven threads of different types. Cloth appearance can vary from matte diffuse to highly specular and anisotropic. Existing models for simulating cloth in graphics are either too simplistic to capture this appearance or too complex for practical use.

In this paper we present a practical appearance model for cloth. Our model is based on extensive measurements of the scattered light by

cloth samples as well as individual threads. Based on these measurements, we have developed a simple model for light scattering by threads as well as cloth made of a given weave pattern. Our appearance model simulates cloth at a distance and ignores the appearance of individual threads unlike recent work on cloth [Irawan 2008]. This makes the model significantly simpler and more robust in terms of matching measured data. In addition, our model takes into account the shadowing and masking by the individual threads in the cloth. Our model is easy to control and it can reproduce a wide range of cloth types including linen, silk, polyester, and velvet with varying weaving patterns. We can also, model the appearance of novel physically plausible cloth fabrics. We include measured parameters for these cloth types including the weave patterns for our cloth samples.

2 Previous Work

Rendering cloth has been an active area of research for more than 25 years. The earliest approaches as well as more recent work are based on empirical shading models [Weil 1986; Daubert et al. 2001; Glumac and Doepp 2004], where the primary goal is to achieve believable shading rather than physical accuracy. Microfacet models have been used by Ashikhmin et al. to model satin and velvet [Ashikhmin et al. 2000]. Adabala et al. continued this work by including support for weave patterns [Adabala et al. 2003]. Wang et al. [2008] introduced their own microfacet-based BRDF for modeling spatially-varying anisotropic reflectance using data captured from a single view. While microfacet models can be effective at capturing a complex appearance these models are difficult to control as they depend strongly on the right microfacet distribution function. Since cloth is often anisotropic it is difficult to obtain this distribution from measured data (see Section 7).

Another approach for simulating cloth is based on modeling the structure of the cloth [Xu et al. 2001; Chen et al. 2003; Drago and Chiba 2004]. While these methods can reproduce a wide range of appearances they can be difficult to control. Yasuda et al. [1992] modeled the peculiar gloss seen in cloth by accounting for the internal structure, but assumed a very simplified model of the structure
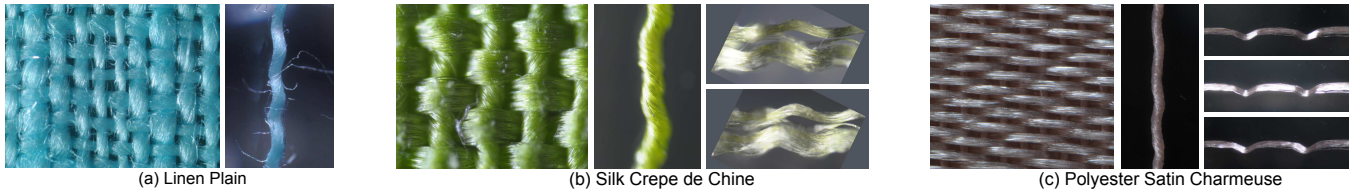
(a) Linen Plain   (b) Silk Crepe de Chine   (c) Polyester Satin Charmeuse

Figure 2: *Microscope pictures of different fabrics.*

and the results lacked verification. Westin et al. [1992] computed BRDFs for velvet and plain weave nylon fabrics through statistical ray tracing of a geometric model of the small-scale cloth structure. Zhao et al. [2011] presented a volumetric rendering approach using CT scanning of cloth fabrics. Their model produces high quality renderings but it is limited to reproducing specific cloth samples.

Irawan et al. developed a comprehensive model for reproducing both the small-scale (BTF) and large-scale (BRDF) appearance of woven cotton cloth [Irawan and Marschner 2006; Irawan 2008]. This model is current state of the art and capable of reproducing a wide range of appearances. The basis of the model is a complex empirical model for light interacting with a cloth thread. This model is evaluated numerically to fit with measured data. The numerical fit is rather costly and to reduce the number of parameters in the model only a specific set of cloth tangents can be accounted for. This limits the accuracy of the model, and it cannot reproduce split highlights as shown in our satin in Figure 13 (d). Furthermore, the model ignores shadowing and masking between different threads of cloth, which limits the accuracy at grazing angles. Finally, the complexity of the model makes it difficult to control in order to achieve a specific appearance (see Section 7).

3 Light scattering from Fabrics

3.1 Acquisition Setup

The cloth measurements presented in this paper were acquired with a fully automatic, four-axis image-based gonioreflectometer. The device consists of two robotic arms, each with two degrees of freedom. Each degree of freedom has a minimum displacement of 0.01 degrees, allowing the arms to move freely to nearly any desired position about the hemisphere which surrounds the measurement platform. In order to capture the data, the outer arm is mounted with a CCD camera and the inner arm is mounted with a light source. In addition to quantitative analysis of cloth reflectance, we investigated different fabric types and their constituent threads under a microscope to gain further intuition about their behavior.

3.2 BRDF Measurements and Observations

Our measurements show that the appearance of cloth is dominated by some combination (in varying amounts) of diffuse reflectance, specular reflectance, shadowing/masking, and grazing angle sheen. While many samples were measured, we focused on three fabrics: Linen Plain, Silk Crepe de Chine, and Polyester Charmeuse. Since each has a unique combination of fiber type, thread structure, and weaving pattern, their measurements provide insight as to which physical characteristics are responsible for the variations in their appearance. The resulting set of observed behaviors produced by these fabrics have not been fully addressed in literature nor have they been validated with ample physical measurements.

3.2.1 Linen Plain

The measured Linen sample is a plain weave fabric assembled with a single type of thread.This particular construction causes the material to look the same both front and back, as well as from perpendicular viewing angles. Under the microscope, as shown in Figure 2 a,
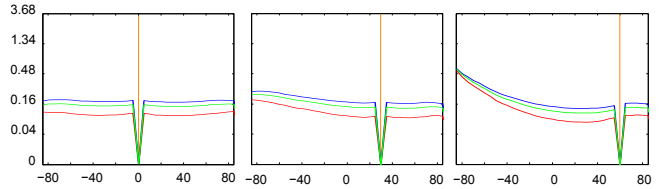
we observe a repeating grid of twisted threads.

Figure 3: *BRDF measurements for Linen Plain for 0°, 30°, and 60° incident angles.*

Due to its orthogonally symmetric structure, linen was measured in only one direction. Figure 3 shows the normal plain BRDF measurements of this fabric along one of its threads. The orange line indicates the direction of incident light. The drop in the plots are due to the occlusion of the light source by the camera. The measurements confirm that linen produces a smooth reflection with no specular peaks under most lighting conditions, except when the fabric is observed at a grazing angle and the light is also grazing. As seen in Figure 3 (right), at these grazing angles, reflectance increases substantially. The measurements also show that the effect of shadowing/masking, manifested by dips at the plot edges, is minimal.

3.2.2 Silk Crepe de Chine

The measured Silk Crepe de Chine sample is assembled with two different types of thread (Figure 2 b). The first type of thread is made of densely twisted fibers. This thread remains straight and uniformly spaced in the fabric. The second type of thread is made of thin and untwisted fibers, and passes above and below the first type. This thread exhibits sharp surface reflection and very little absorption resulting in its translucent appearance. While moving a light around the microscope, a strong specular reflection in two incidence directions is visible.The variation in thread type as well as the weaving pattern structure result in an asymmetrical surface which causes this fabric to appear significantly different in perpendicular viewing directions. To demonstrate this, two perpendicular planes of silk were measured (Figure 4). Measurements in the plane parallel to the flat threads (top row) show two off-specular peaks, while the perpendicular plane measurements (bottom row) exhibit two grazing angle peaks. Furthermore, the parallel measurements clearly indicate a drop in reflectance as the eye approaches grazing angle, suggesting the contribution of shadowing/masking. In contrast, the perpendicular measurements maintain the grazing angle peaks under all lighting conditions.

3.2.3 Polyester Satin Charmeuse

The measured Polyester Satin Charmeuse sample is a satin weave fabric, meaning that the threads in one direction cross over most of the threads in the other direction. Like Silk, this fabric is made out of two distinct (polyester) threads. The flat threads go above and below the twisted threads, but remain longer above than below. This asymmetry in the weaving pattern causes the fabric to have two different sides (Figure 2 c). While moving the light around the microscope, we noticed strong reflections in three different direction of light.The variation in thread type and the asymmetric weaving pattern result in strong anisotropic reflectance. The fabric was
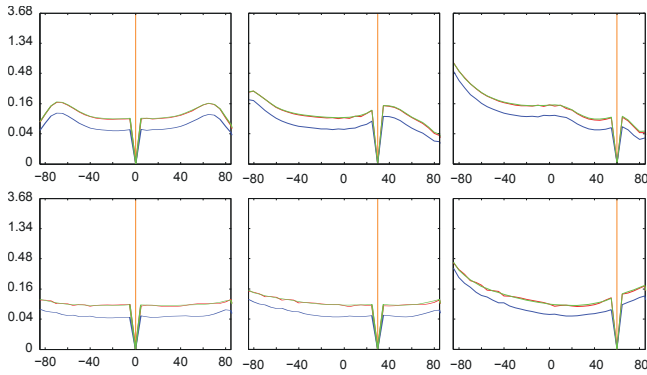
Figure 4: *BRDF measurements for Silk Crepe de Chine for 0°, 30°, and 60° incident angle. The top row corresponds to the in plane measurements parallel to the direction of flat threads, and the bottom row represents the measurements in the perpendicular direction.*

measured in two perpendicular planes (Figure 5). In plane measurements along the direction of flat threads exhibit three specular peaks, one in the reflection direction and the other two in equal but opposite off-specular directions. Measurements in the perpendicular plane exhibit grazing angle peaks which are visible under all lighting conditions.
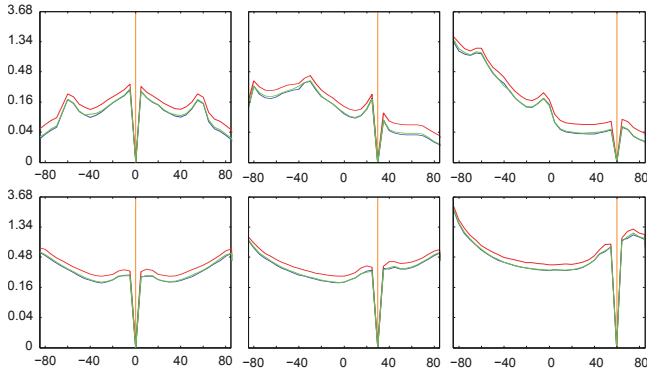

Figure 5: *BRDF measurements for Polyester Charmeuse for 0°, 30°, and 60° incident angles. Top row corresponds to in plane measurements along the direction of flat threads, and the bottom row represents measurements in the perpendicular direction.*

4 Light Scattering from Threads

In the previous section we noted that the there are two different types of threads that contribute to the overall appearance of cloth fabrics. The first and most common type of threads are densely twisted threads. These threads have many varieties that differ by twist level and constituent fiber count. The twist level of threads affects the compactness and density of fibers that compose them [Saville 1999]. The second type of threads have a minimal amount of twist in their construction and we will refer to them as flat threads. These are usually less dense and have a greater diameter due to their loosely packed structure. Both thread categories are fed by a diverse selection of raw materials such as silk, cotton, wool, flax, and synthetic filaments. We further investigate the light scattering properties of cloth fabrics by measuring the BRDF of individual threads of different type.

4.1 Acquisition Setup

We measured the radiance distribution of several thread types using the same spherical gantry as used for the cloth measurements and a unique suspension apparatus. The results served to validate our analytical model as well as provide a qualitative basis for reasoning about threads and cloth in general. In our measurements we illuminate an 8 cm section of thread with a collimated light beam and collect radiance scattering measurements with a CCD camera.

To procure a thread sample, we first remove a single strand from a finished fabric. When a thread is removed from fabric it is no longer straight, but retains the shape that it had in the fabric. In order to obtain accurate scattering measurements, the thread must be extended to its maximal length. This type of procedure is common in fabric quality testing and requires standard tension, which has the general goal of non-destructively pulling on one end of the thread. In our experimental thread mount, we clamp one end of the thread to a poseable arm, and let the rest of it hang, weighed down by a magnetic set of spheres at the unclamped end. Hanging the thread in mid-air allows the gantry to measure a full 4D BRDF with minimal occlusions and no background to contaminate the measurements. Additionally, gravity provides a vertically straight thread orientation which eliminates pose calibration.

4.2 BRDF Measurements

We measured a complete 3D BRDF by varying the longitudinal angles θ_i, θ_r, and the azimuthal difference angle $\phi_d = \phi_i - \phi_r$. Figure 7 shows the notations used in our paper. We did not measure a 4D BRDF because we assumed symmetry of the BRDF with respect to ϕ. Since threads are not perfect cylinders, this assumption is somewhat violated, however, it allows us to capture less data while still observing the salient thread scattering features. We present a planar slice of the resulting measurements in Figure 6. Here the BRDF is a function of two angles θ_i and θ_r). We present several θ_i angles and plot a continuous range of BRDF measurements for θ_r. The threads were not treated with any dyes and no polarizing filters were used. As a result, the BRDF plots represent the natural visible combination of surface reflection and internal scattering. To facilitate intuition about the plots we can state the following: surface reflection results in a lobe in the specular reflection direction ($\theta_r = -\theta_i$), and internal scattering results in a wider lobe that is more decoupled from appearing in the specular direction. The top row of Figure 6 demonstrates the similarity among
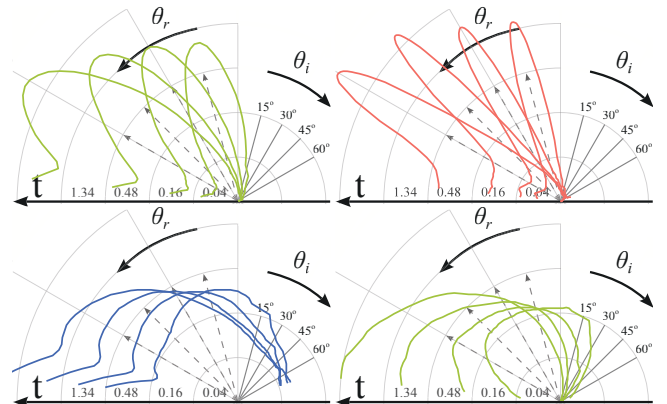

Figure 6: *Polar plots of measured incidence plane BRDF for different threads. Each quadrant of the figure contains the rgb average BRDF for a thread type. Starting at the top row, and moving left to right we have flat silk thread, flat polyester thread, twisted linen thread, and twisted silk thread.*

flat threads and their disparity from twisted threads. In the top row,

both the polyester and the silk thread possess narrow specular lobes oriented at the exact specular reflection direction. This result can be attributed to their low surface roughness as well as minimal internal scattering. The fact that the lobe is oriented at the exact specular reflection direction means that, unlike hair, threads have no consistent cuticle that displaces their specular reflection. The polyester thread is the more specular of the two flat threads, as evidenced by its narrower and brighter reflection lobe. This can be attributed to the synthetic vs. organic fibers that they are composed of, where polyester has fewer natural imperfections and irregularities due to its industrial fabrication process.

At first glance the twisted threads in the bottom row of Figure 6 appear nearly identical. They both exhibit a characteristic wide scattering lobe that slowly increases as the light goes to glancing angle. Focusing on glancing incidence angles, we observe that the twisted linen thread scatters more light in the non-specular directions. This type of BRDF can be attributed to either a very rough surface or isotropic internal scattering. We address these behaviors in subsequent sections when we present our thread BRDF model.
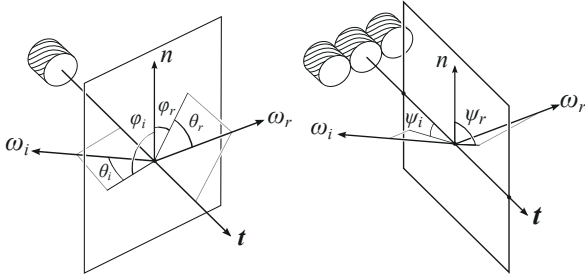

Figure 7: *Notations and geometry of light reflection from a cylindrical fiber. (right) Longitudinal angles θ are computad with respect to the normal plane and the azimuthal angles φ are computed based on the local surface normal direction n. When the thread is not part of a fabric n can be any arbitrary direction within the normal plane. (left) Longitudinal angles ψ_i and ψ_r are the angles between local surface normal n and the projection of ω_i and ω_r on to the plane spanned by t and n vectors.*

4.3 A Light Scattering Model for Threads

Based on our measurements of individual threads, we observed an optical behavior that is similar to hair and more generally, smooth dielectric cylinders. We observed that the reflection of a collimated light beam from a taut thread sample forms a cone centered on the thread axis. Additionally, the surface reflection is framed by a subtle color reflection that is also centered at the cone. This type of reflection from cylinders has been previously studied by [Kajiya and Kay 1989; Kim 2002; Marschner et al. 2003], where the normal plane around the tangent is used as the coordinate frame for computing light scattering behavior. Unlike hair, threads do not have tilted cuticles on their surface and therefore the reflected rays will stay on the reflection cone regardless of the number of bounces inside the thread. In our model we abstract the thread geometry and

f_s	Thread scattering function
F_r	Fresnel reflectance
F_t	Fresnel transmittance
γ_s	Surface reflectance Gaussian width
γ_v	Volume scattering Gaussian width
k_d	Isotropic scattering coefficient
A	Colored albedo coefficient

Table 1: *Description of important symbols.*

optical behavior with a cylinder. When a beam from ω_i consisting

of parallel rays of light strikes a thread cylinder running along the vector t, each ray in the beam reflects at the surface according to the surface normal of the cylinder. These surface normals are all perpendicular to the thread tangent vector t and lie in the normal plane. For a smooth specular cylinder, a beam incident at θ_i will be reflected in the ideal specular direction $-\theta_i$ across the normal plane and, due to the circular cross section of the cylinder, will be spread into a cone [Kajiya and Kay 1989]. The refracted light will enter the cylinder and after any number of internal reflections and refraction will emit into the same cone as the surface specular reflection [Marschner et al. 2003].

To establish radiometric notation for our cylinder based model we use the curve radiance integral from [Marschner et al. 2003]:

$$L_r = \int f_s(t, \omega_i, \omega_r) L_i(\omega_i) \cos \theta_i \, d\omega_i \qquad (1)$$

Note that unlike the standard radiance integral on a surface, the reflected radiance from a cylinder differs by the fact that it is defined over a unit length instead of a unit area. This difference arises from the fact that the cylinder scattering function accounts for all the light scattered around the circumference of the cylinder.

As in previous treatments of BSDFs [Hanrahan and Krueger 1993], we separate our scattering function $f_s(t, \omega_i, \omega_r)$ into a surface scattering component $f_{r,s}$, and volume scattering component $f_{r,v}$. In addition to the angles in Figure 7, we introduce $\phi_d = \phi_i - \phi_r$ and $\theta_h = (\theta_i + \theta_r)/2$ to define the two scattering functions.

4.3.1 Surface Reflection

We model surface reflection similarly to [Marschner et al. 2003], except we do not decompose our computation into longitudinal and azimuthal planes.

$$f_{r,s}(t, \omega_i, \omega_r) = F_r(\eta, \vec{w_i}) \cos(\phi_d/2) g(\gamma_s, \theta_h) \qquad (2)$$

The $\cos(\phi_d/2)$ term arises due to projection of the circular cylinder cross-section, as demonstrated by [Kim 2002], and previously used by [Sadeghi et al. 2010] for hair rendering. To break away from the idealized smooth cylinder representation of threads, we employ a unit area Gaussian g with width γ_s to simulate surface roughness. Finally, we add physical accuracy to the model by attenuating the power by a Fresnel term. The actual angle used to compute the Fresnel term is based on the reflection normal on the cylinder as well as a half-angle between the light and the eye, yielding an exact expression $F_r(\eta, \cos^{-1}(\cos(\theta_d) \cos(\phi_d/2)))$, where $\theta_d = (\theta_i - \theta_r)/2$. This model produces a glossy reflection on a cone around the thread with physical and geometric attenuation. We considered using the full micro-facet specular formulation, but found that it did not improve matching to our measured results.

4.3.2 Volume Scattering

Real threads are composed of fibers that are either twisted together or lay flat next to each other. We make a unifying assumption that all fiber types are cylindrical with minimal eccentricity. This is generally true with the exception of cotton, which resembles a flat ribbon. To summarize, our model is a large thread cylinder composed of tiny fiber subcylinders. This enables us to use the fact that smooth cylinders emit light due to internal scattering into the ideal reflection cone. Therefore, light that enters the thread volume and undergoes any type of scattering interaction with the fiber subcylinders will result in a surface emission into the same cone as the surface reflection. One thing to note is that the orientation of the fiber subcylinders differs from that of the thread cylinder. We model this deviation as a normal distribution centered on the thread tangent. Therefore, a flat thread will have a much smaller variance

than a twisted thread. We model these behaviors while maintaining physical constraints in the following equation:

$$f_{r,v}(t, \omega_i, \omega_r) = F \, \frac{(1 - k_d) \, g(\gamma_v, \theta_h) + k_d}{\cos \theta_i + \cos \theta_r} \, A \qquad (3)$$

Here $F = F_t(\eta, \vec{w_i})F_t(\eta', \vec{w_r'})$ is the product of two transmission Fresnel terms. We define the subcylinder tangent deviation with a Gaussian lobe g with width γ_v. The Gaussian lobe controls the width the forward scattering cone. For twisted threads, which consist of fibers that deviate from the thread tangent direction, this Gaussian is wider than for flat threads which mainly consist of parallel filaments. Additionally, we define a tunable isotropic scattering term k_d and a color albedo term A. We added an isotropic scattering term to account for cellulose based fibers such as cotton and linen, which predominantly yield isotropic volume scattering instead of a forward scattering cone. The division by the sum of projected cosines comes from [Chandrasekhar 1960], in his derivation for diffuse reflectance due to multiple scattering in a semi-infinite medium. Adding this normalization term gave us better matches with our measured results. The complete thread scattering model is a sum of the surface and volume components:

$$f_s(t, \omega_i, \omega_r) = \big(f_{r,s}(t, \omega_i, \omega_r) + f_{r,v}(t, \omega_i, \omega_r)\big)/\cos^2 \theta_d \quad (4)$$

Note that the complete scattering formulation contains a division by $cos^2\theta_d$, which is necessary to account for the solid angle attenuation of the specular cone [Marschner et al. 2003]. Previous work has addressed volume scattering in threads with a cylindrical phase function in [Irawan 2008] as well as the Henyey-Greenstein phase function in [Adabala et al. 2003]. We experimented with various phase functions as well, but found them inadequate due to their decoupled behavior from the direction of the thread. Our approach is similar in spirit to [Jakob et al. 2010], which defines phase functions oriented to the direction of fibers to achieve highly anisotropic volume scattering.

We have defined a complete BSDF for individual threads, which matches well to our measured results. It was our goal to define as few non-physical control parameters as possible to enable the physical and geometric scattering constraints to drive its behavior. We note that the model is only suitable for distant viewing of threads since it assumes that the rays of light incident on the thread cylinder are parallel and that the thread is locally straight.

4.4 Matching Measured BRDFs

In this section we provide evidence for the validity of our model by comparing it to measured BRDFs of thread. We accomplish this by manually fitting our model parameters to measured results. We did not consider automatic fitting approaches due to the minimal number of control parameters and their predictable nature.

In Figure 8, we demonstrate the performance of our model with measured BRDF results in the top row and our model in the bottom row. Each row shows BRDF measurements for three incident light angles of two thread types: one twisted, and one flat. The first three plots in each row correspond to a twisted polyester thread extracted from the Polyester Satin Charmeuse cloth sample. Our model results in the bottom row are able to closely match the measured results in the top. We achieve this by observing a wide surface reflectance Gaussian supplemented by an even wider volume Gaussian and a red tinted albedo coefficient.

The second set of three plots in Figure 8 correspond to a flat polyester thread from the same cloth sample. Our model closely simulates the scattering profile of this thread by setting a very narrow surface reflectance Gaussian and a small red tinted albedo. Our model is validated by being able to closely simulate the scattering

behavior of different thread types under various incident light angles.

5 An Appearance Model for Cloth

We consider cloth fabric as a mesh of interwoven smooth cylinders oriented in two orthogonal directions. These cylinders, which we will refer to them as microcylinders, are considered to be very small compared to the geometry of the fabric. We use texture UV coordinates of the mesh as the direction of microcylinders but any other direction can be used. As discussed in section 4.3, we do not rely on a specific surface normal in our cylinder scattering model and therefore need only tangent directions at the cloth level (Section 5.1). However, the surface normal does come into play in shadowing/masking calculations (Section 5.2).

5.1 Shading Model

In order to render cloth fabrics, we evaluate the outgoing radiance from the *smallest patch* of the weaving pattern. This patch is the smallest portion of the weaving pattern which has the following property: the complete weave can be constructed by repeating this patch. Note that the smallest patch is not unique since all of them contain the same set of tangents even though they come from different threads (see Figure 10 left). We assume that the smallest patch is locally flat and smaller than a pixel in the image plane. Additionally, for clarity, we constrain our discussion to cloth patches that contain exactly two threads, one orthogonal to the the other, as is common in most weaving patterns. However, the formulations in this section can be trivially extended to compute the contribution from any number of threads in a smallest patch. We define the outgoing radiance of the smallest patch to be the weighted average of the outgoing radiance of constituent threads based on their local orientation and coverage inside the smallest patch (See Figure 9):
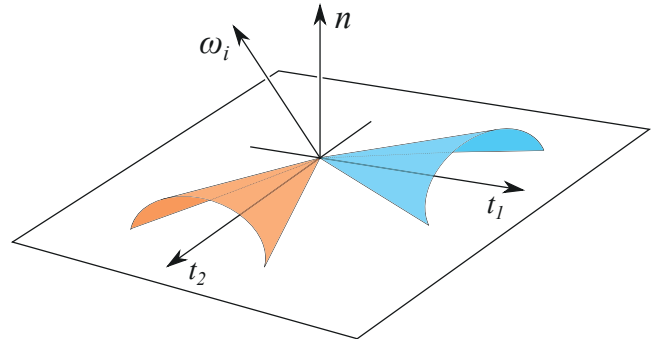

Figure 9: *Our shading model treats the fabric as a mesh of microcylinders oriented in two orthogonal directions.*

$$L_r(\omega_r) = a_1 \times L_{r,1}(\omega_r) + a_2 \times L_{r,2}(\omega_r) \qquad (5)$$

where a_1 and a_2 represent the area coverage ratio of the first and second thread within the smallest patch respectively. If the weaving pattern has no empty spaces, these two numbers add up to one.

For each thread, we define a *tangent curve* that describes its tangent distribution inside the smallest patch (Figure 10 right). We specify the tangent curve by setting the tangent values at discrete control points. In order to compute the total radiance of each thread, we sample its corresponding tangent curve at T equidistant points and compute a weighted radiance contribution of the samples according
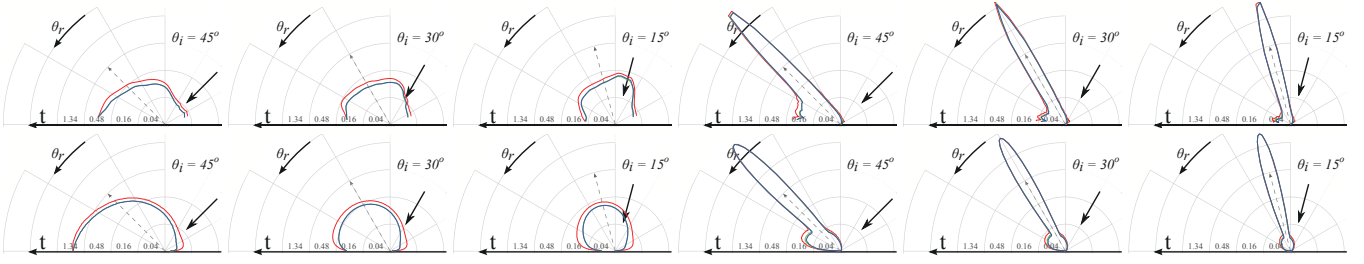
Figure 8: *Incidence plane thread BRDF measurements in the top row matched by thread model in the bottom row. In each row the first three plots are for a twisted thread and the last three for a flat thread. The two threads were extracted from the same Polyester Satin Charmeuse cloth sample. The plots show scattering as a function of view angle.*

to the following formula:

$$L_{r,j}(\omega_r) = \int \frac{\sum_{t \in C_j} f_s(t, \omega_i, \omega_r) L_i(\omega_i) \cos \theta_i}{2\,T}\, d\omega_i$$

$$= \frac{1}{2\,T} \int L_i(\omega_i) \Big(\sum_{t \in C_j}^{T} f_s(t, \omega_i, \omega_r) \cos \theta_i \Big)\, d\omega_i \quad (6)$$

where j can be either 1 or 2 and represents the thread direction, C_j is the set that contains the T sampled tangents from the tangent curve of the corresponding thread, and f_s is the analytical thread BSDF model introduced in Section 4.3 . We are dividing by $2\,T$ since there are T tangent samples for each direction of threads.
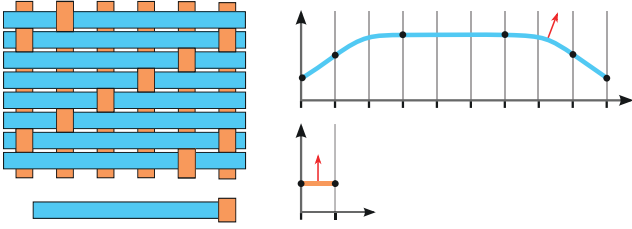

Figure 10: *The weaving pattern and a sample tangent curve for the Polyester Satin Charmeuse fabric: (left top) the weaving pattern, (left bottom) a smallest patch, (right) the tangent curve for the two types of threads. The red arrows indicate the local normal of the tangent which is used in the shadowing and masking calculations.*

5.2 Shadowing and Masking

Shadowing and masking are very important for the correct evaluation of the outgoing radiance especially at grazing angle viewing and lighting directions. Poulin and Fournier [1990] derived a shadowing and masking term for grooved surfaces composed of cylinders. However, their approach is not applicable to our model since they assumed that the cylinders have a surface patch BRDF and integrated all of the reflected light scattered toward a viewer. Since our formulation treats cylinders as one-dimensional entities, we do not compute the explicit reflectance variation across their circumference.

Shadowing and masking are very similar concepts; shadowing can be thought of as masking from the point of view of the light source. We interchangably refer to both of these quantities as masking M in the rest of this section. We only compute the masking between the same types of threads (i.e. threads with same overall directions). Shadowing between threads with different orientations is more involved and is left as future work.

Consider the setup shown in Figure 11 where the fabric is wrapped around a cylinder. Let us first focus on the horizontal threads only (Figure 11 middle). Threads along this direction never occlude each

other from the viewer even at grazing angles. Therefore, the cylinder BSDF defined in Section 4.3 alone can be used to compute the correct outgoing radiance from these types of threads with no masking adjustment. Now let us consider the vertical threads (Figure 11
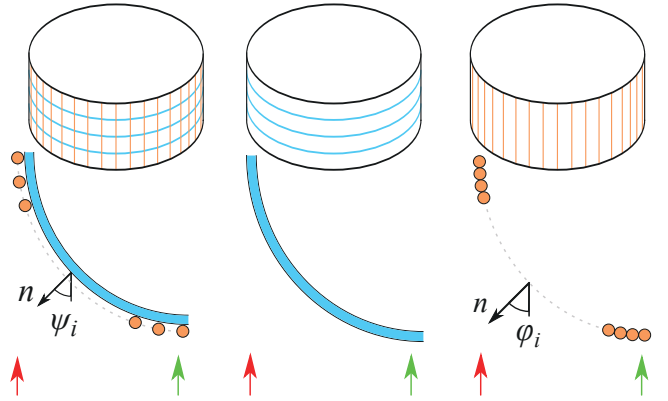

Figure 11: *Fabric as two different directions of threads with views from above (green arrows) and from grazing angles (red arrows): (left) The contribution of different threads in the smallest patch is related to the orientation of the patch. At grazing angles, the blue thread contributes less than the orange thread. (middle) In the longitudinal direction, there is no masking and no adjustment needed.(right) In the azimuthal direction, the amount of masking in grazing angles is dependent on the $\cos \phi_i$.*

right). At grazing angles each thread partially masks the thread behind it and gets masked by the thread in front of it. The amount of masking is relative to the cosine of the viewing direction projected to the thread normal plain and the surface normal. This angle is equal to ϕ_i (see Figure 7).

$$M(t, \omega_i) = \max(\cos \phi_i, 0) \quad (7)$$

If the cosine is negative, the surface is a backface and is being self-masked. The same argument holds for the light direction and results in shadowing.

$$M(t, \omega_r) = \max(\cos \phi_r, 0) \quad (8)$$

Here ϕ_i and ϕ_r are computed with respect to the local normal of the tangent t. If the tangent deviates from the surface tangent by α degrees then its normal will deviate from the surface normal by α degrees as well. See Figure 10 for an illustration.

When ω_i and ω_r are not correlated, the overall shadowing and masking amount is equal to the multiplication of $M(t, \omega_i)$ and $M(t, \omega_r)$. In cases where these two directions are close to each other (e.g. driving at night), we use the adjustment introduced by Ashikhmin et al. [2000] to compute the overall shadowing and

masking term $M(t, \omega_i, \omega_r)$:

$$
\begin{aligned}
M(t, & \omega_i, \omega_r) = \\
& (1 - u(\phi_d))\, M(t, \omega_i) \times M(t, \omega_r) + \\
& u(\phi_d)\, \min(M(t, \omega_i), M(t, \omega_r))
\end{aligned}
\tag{9}
$$

where u is a unit height Gaussian function with standard deviation between 15° and 25° [Ashikhmin et al. 2000]. We will refer to $M(t, \omega_i, \omega_r)$ in short as $M(t)$. We can rewrite Equation 6 to include the effect of shadowing and masking:

$$
\begin{aligned}
L_{r,j}(\omega_r) & = \\
& \frac{1}{2T} \int L_i(\omega_i) \Big(\sum_{t \in C_j} f_s(t, \omega_i, \omega_r) M(t) \cos \theta_i \Big) \, d\omega_i.
\end{aligned}
\tag{10}
$$

To see the effect of shadowing and masking see Figure 17.

5.3 Reweighting

So far we have considered that the contribution of a tangent to the overall reflection of the smallest patch is based on its length (i.e. area coverage). This is only correct when the ω_r and ω_i are near surface normal n. We need to adjust the contribution of each tangent t based on its projected length $P(t, \omega_i)$ onto the image plane. Tangents that are more visible inside the smallest patch will have a higher contribution (for that viewing angle). We refer to this adjustment as reweighting. This process determines the contribution of each tangent curve sample to the overall reflectance of the smallest patch.

Projection of the tangents onto the image plane is based on the cosine of the longitudinal angle ψ_i. As shown in Figure 7, ψ_i is the angle between local surface normal n and the projection of ω_i on to the plane that contains t and n.

$$
P(t, \omega_i) = \max(\cos \psi_i, 0)
\tag{11}
$$

When the cosine is negative, the tangent is being self-masked and contributes zero to the overall reflection of the patch. Similar to the masking term, we calculate the projection for both ω_i and ω_r directions. This means that tangents receive energy based on their visibility from the point of view of the light source. We combine these two projections to get the final projection term $P(t, \omega_i, \omega_r)$:

$$
\begin{aligned}
P(t, & \omega_i, \omega_r) = \\
& (1 - u(\psi_d))\, P(t, \omega_i) \times P(t, \omega_r) + \\
& u(\psi_d)\, \min(P(t, \omega_i), P(t, \omega_r))
\end{aligned}
\tag{12}
$$

where ψ_d is the difference between ψ_i and ψ_r. We refer to $P(t, \omega_i, \omega_r)$ in short as $P(t)$. Finally we can rewrite Equation 10 to get our complete shading model:

$$
\begin{aligned}
L_{r,j}(\omega_r) & = \\
& \int L_i(\omega_i) \Big(\frac{\sum_{t \in C_j} f_s(t, \omega_i, \omega_r) M(t) P(t) \cos \theta_i}{\sum_{k \in C} P(k)} \Big) \, d\omega_i.
\end{aligned}
\tag{13}
$$

where $C = C_1 \cup C_2$ is the set that contains $2\,T$ sampled tangents from the tangent curves of both threads. To see the effect of reweighting on the final result see Figure 17.

6 Results

We have implemented the cloth model in a ray tracer and on the GPU. This section contains rendered results for several different cloth fabrics. The parameters for each cloth sample is summarized in Table 2 and the tangent distribution is given in Appendix A.

We have matched our rendered results against photographs. To capture the anisotropic behavior of different fabrics, we have wrapped the fabrics around a cylinder in three different directions. We label each mode based on the orientation of the flat threads as vertical, horizontal, and diagonal (see Figure 12). For the Linen Plain fabric, the vertical and horizontal modes are identical. For comparison, we present our rendered results of different fabrics in the same setup.
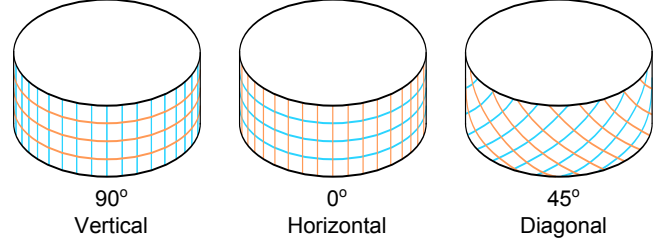

| 90° | 0° | 45° |
| Vertical | Horizontal | Diagonal |

Figure 12: *To capture the anisotropic behavior of different fabrics, we have wrapped the fabric around a cylinder in three different orientations where the flat threads stay (left) vertical, (middle) horizontal, and (c) diagonal.*

Figure 13 shows our results comparing photographs of Linen Plain, Silk Crepe de Chine, and Polyester Satin Charmeuse fabrics against our rendered results. Note, how our model is able to capture the variation in the highlights across the different fabrics including the grazing angle highlight seen on the silk, and the split highlight seen on the backside of the Satin (note, that the cloth is also illuminated from the backside). The back side of this fabric has a different appearance due to an asymmetry of the weaving pattern. It can be seen from the first two columns that all four cloth samples show anisotropic behavior (even slightly visible for the linen), and our model is able to not only capture this, but also accurately predict the appearance when the cloth sample is rotated 45 degrees.

Figure 14 show a comparison of our BRDF with the measured BRDF of the fabric (Figure 14 top) for the front side of the fabric and along the direction of flat threads. Note, how the model is able to capture the variation in the location of the highlights and the overall shape of the reflected light as the light source moves from normal incidence to 30 and 60 degrees.
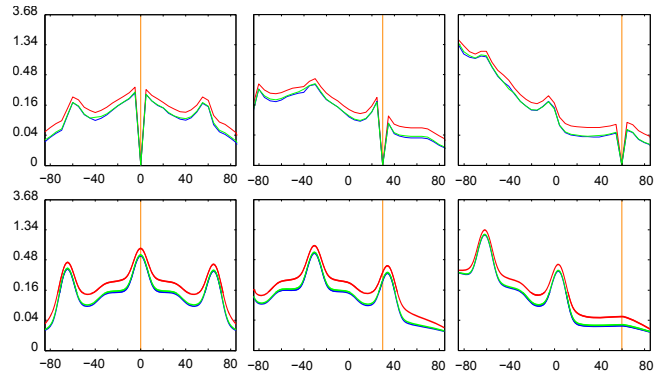

Figure 14: *Matching a BRDF measurement of the Polyester Satin Charmeuse fabric with our model. (top) normal plain BRDF measurement of the front side of Polyester Satin Charmeuse fabric along the direction of flat threads compared to (bottom) the result of our appearance model.*

Figure 15 demonstrates how our model can reproduce the appearance of other fabrics that have been previously studied. We have successfully matched a Silk Shot Fabric (presented in [Pont and Koenderink 2003]) and a Velvet fabric (presented in [Ashikhmin 2001]). The Silk Shot fabric is composed of threads with two dif-

Fabric	η	Thread	A	k_d	γ_s	γ_v
Linen Plain	1.46	Both	$(0.2, 0.8, 1) \times 0.3$	0.3	12	24
Silk	1.345	Flat	$(1, 0.95, 0.05) \times 0.12$	0.2	5	10
Crepe de Chine		Twisted	$(1, 0.95, 0.05) \times 0.16$	0.3	18	32
Polyester	1.539	Flat	$(1, 0.37, 0.3) \times 0.035$	0.1	2.5	5
Satin Charmeuse		Twisted	$(1, 0.37, 0.3) \times 0.2$	0.7	30	60
Silk	1.345	Dir 1	$(0.1, 1, 0.4) \times 0.2$	0.1	4	8
Shot Fabric		Dir 2	$(1, 0, 0.1) \times 0.6$	0.1	5	10
Velvet	1.46	Both	$(0.05, 0.02, 0) \times 0.3$	0.1	6	12

Table 2: *The list of parameters obtained from our measured cloth samples. The γ parameters are measured in degrees.*
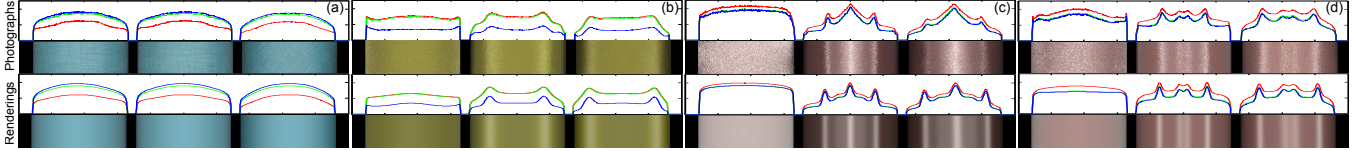

Figure 13: *Photograph and the rendered results for (a) Linen Plain, (b) Silk Crepe de Chine, (c) front side of Polyester Satin Charmeuse, and (d) back side of Polyester Satin Charmeuse. The three cylinders show three cloth orientations as illustrated in Figure 12.*

ferent colors (in this case red and green) resulting in a complex anisotropic appearance. Our model we can reproduce this appearance using anisotropic volume scattering by the colored threads rather than the shadowing and masking effect as it was assumed by Pont and Koenderink [Pont and Koenderink 2003]. Our model can easily reproduce the appearance of Velvet (see Figure 16) by setting the tangent distribution to be near perpendicular to the surface of the fabric.

Figure 15: *Comparison between photographs (top row) and rendered samples (bottom row) for (left) Silk Shot Fabric (from [Pont and Koenderink 2003]) and (right) Velvet Fabric (from [Pont and Koenderink 2003]). In both cases only the vertical and horizontal mode were available and our model is predicts the appearance for the diagonal mode.*

Velvet fabric, we are using a texture map to specify the groom direction. We also rendered two imaginary cloth fabrics: one is a weaving of silk and polyester threads using a Shantung weaving pattern and the other is using an imaginary fabric with asymmetric specular peaks.

Figure 17 shows the effect of shadowing and masking as well as the reweighting process. Note the bright edges in the vertical mode which are the results of the contribution of all vertical flat fibers at grazing angles. The masking term corrects this effect by reducing the intensity of masked threads in grazing angles. The reweighting process intensifies the amount of contribution of the threads based on their projected length on to the image plane (or light plane). For example in the vertical mode, the flat threads will occupy more area of the smallest patch than the twisted threads at grazing angles. Therefore they will contribute more in those cases.

Figure 17: *The effect of shadowing and masking and the reweighting process on the final results: (a) the result for the shading model, (b) the effect of shadowing/masking term, and (c) the final results after applying shadowing/masking and reweighting.*

The images in Figure 16 have been rendered in 512×512 resolution with 144 samples per pixel in an unoptimized CPU ray tracer. The renderings took 51 minutes on average on an 2.83 GHz Intel Core 2 CPU. We have implemented the same model in a GPU shader. The images in Figure 18 were rendered in 100 ms. on a laptop with an Intel I5 M480 processor and a mobile NVIDIA GT420 GPU.
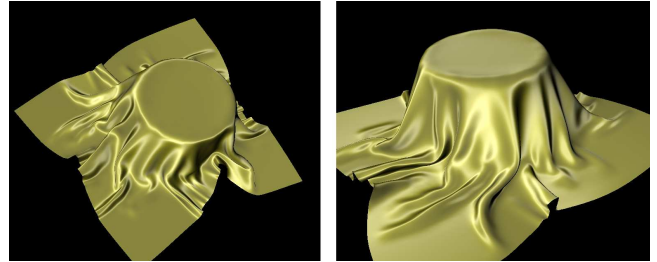

Figure 18: *Screenshots from the GPU implementation of our model. Each image was rendered in roughly 100 ms on a mobile GT420 GPU.*

7 Discussion

As shown in the results, our model is able to reproduce the complex behavior of a variety of fabrics. Our appearance model is based on our analytical thread BSDF model for different types of thread and the tangent distribution of threads in a weaving pattern. Our work is similar to the model of Ashikhmin et al. [2000] in the sense that they can reproduce a specular reflection in any direction by distributing the microfacets in the appropriate direction. We reproduce specular peaks by orienting the tangents so that their reflection cone lies in the desired direction. The input of our model is intuitively based on the weaving pattern of the fabric, while their model requires a complicated mathematical representation of the surface normals. For example, for producing the appearance of Velvet fabric, Ashikhmin et al. propose $c \times \exp(-\cot^2 \theta/\sigma^2)$ to be the distribution of normals (where c and σ are control parameters). Formulating with the correct equation can be a challenging task. In our model we define the tangents to be almost perpendicular to the surface normal and we can reproduce the appearance of Velvet.

A limitation of our model in its current form is that it cannot accurately produce close-up renderings. It does not reproduce the appearance of single threads in a patch, or the reflectance variation across each thread, assuming that the smallest patch of the fabric is smaller than a pixel in the image plane. This limitation can be

Figure 16: *Our rendered results for different fabrics. From top to bottom, left to right: Linen Plain, Silk Crepe de Chine, front side of Polyester Satin Charmeuse, back side of the Polyester Satin Charmeuse, Silk Shot Fabric, Velvet, an imaginary fabric made out of silk and polyester threads with a Shantung weaving pattern, and an imaginary fabric with asymmetric specular peaks.*

somewhat worked around with a texture, but a texture will fail for extreme close-ups, where it will be necessary to model actual geometry such as [Zhao et al. 2011]. Additionally, our shadowing and masking term does not handle masking between threads with orthogonal directions. This causes an underestimation of masking at extreme grazing angles. Finally, our model ignores the effect of multiple scattering between different threads.

8 Conclusion and Future Work

We have presented a practical appearance model for cloth fabrics. Our model is simple and efficient and can be used to reproduce the complex anisotropic appearance of cloth. We present both measurements and a novel scattering model for threads. We use this model to render cloth fabrics. Our cloth BRDF is based on the tangent distribution of interwoven threads, and it includes shadowing and masking terms that are important for grazing angle viewing and lighting. Our model has intuitive inputs and can run in real-time on a GPU.

One avenue for future research is investigating the shadowing and masking between threads with different directions. In addition, we are interested in testing automated fitting processes to estimate the parameters of our model based on photographs of a cloth fabric wrapped around a cylinder in different directions. Furthermore, we aim to investigate the transmission term and approximate the multiple scattering of light between different threads. Lastly, it would be interesting to investigate different ways of importance sampling our fabric BRDF.

References

ADABALA, N., MAGNENAT-THALMANN, N., AND FEI, G. 2003. Visualization of woven cloth. In *Proceedings of the 14th Eurographics workshop on Rendering*, Eurographics Association, Aire-la-Ville, Switzerland, Switzerland, EGRW '03, 178–185.

ASHIKHMIN, M., PREMOŽE, S., AND SHIRLEY, P. 2000. A microfacet-based brdf generator. In *Proceedings of the 27th annual conference on Computer graphics and interactive techniques*, ACM Press/Addison-Wesley Publishing Co., New York, NY, USA, SIGGRAPH '00, 65–74.

ASHIKHMIN, M. V. 2001. *Approximate methods for improving surface appearance*. PhD thesis. AAI3012256.

CHANDRASEKHAR, S. 1960. *Radiative Transfer*. Dover Publications.

CHEN, Y., LIN, S., ZHONG, H., XU, Y.-Q., GUO, B., AND SHUM, H.-Y. 2003. Realistic rendering and animation of knitwear. *IEEE Transactions on Visualization and Computer Graphics 9*, 1, 43–55.

DAUBERT, K., LENSCH, H. P. A., HEIDRICH, W., AND SEIDEL, H.-P. 2001. Efficient cloth modeling and rendering. In *Proceedings of the 12th Eurographics Workshop on Rendering Techniques*, Springer-Verlag, London, UK, 63–70.

DRAGO, F., AND CHIBA, N. 2004. Painting canvas synthesis. *Vis. Comput. 20*, 5, 314–328.

GLUMAC, R., AND DOEPP, D. 2004. Generalized approach to rendering fabric. In *ACM SIGGRAPH 2004 Sketches*, ACM, New York, NY, USA, SIGGRAPH '04, 120–.

HANRAHAN, P., AND KRUEGER, W. 1993. Reflection from layered surfaces due to subsurface scattering. In *Proceedings of the 20th annual conference on Computer graphics and interactive techniques*, ACM, New York, NY, USA, SIGGRAPH '93, 165–174.

IRAWAN, P., AND MARSCHNER, S. 2006. A simple, accurate texture model for woven cotton cloth. Tech. rep., Cornell University, Department of Computer Science.

IRAWAN, P. 2008. *Appearance of woven cloth*. PhD thesis, Ithaca, NY, USA. AAI3295837.

JAKOB, W., ARBREE, A., MOON, J. T., BALA, K., AND MARSCHNER, S. 2010. A radiative transfer framework for rendering materials with anisotropic structure. *ACM Trans. Graph. 29* (July), 53:1–53:13.

KAJIYA, J. T., AND KAY, T. L. 1989. Rendering Fur With Three Dimensional Textures. In *Computer Graphics (Proceedings of SIGGRAPH 89)*, ACM, New York, NY, USA, 271–280.

KIM, T.-Y. 2002. *Modeling, Rendering and Animating Human Hair*. PhD thesis, University of Southern California, Los Angeles, CA, USA.

MARSCHNER, S. R., JENSEN, H. W., CAMMARANO, M., WORLEY, S., AND HANRAHAN, P. 2003. Light Scattering from Human Hair Fibers. *ACM Transactions on Graphics 22*, 3, 780–791.

PONT, S. C., AND KOENDERINK, J. J. 2003. Split off-specular reflection and surface scattering from woven materials. *Appl Opt 42*, 8, 1526–33.

POULIN, P., AND FOURNIER, A. 1990. A model for anisotropic reflection. In *Proceedings of the 17th annual conference on Computer graphics and interactive techniques*, ACM, New York, NY, USA, SIGGRAPH '90, 273–282.

SADEGHI, I., PRITCHETT, H., JENSEN, H. W., AND TAMSTORF, R. 2010. An artist friendly hair shading system. *ACM Trans. Graph. 29* (July), 56:1–56:10.

SAVILLE, B. P. 1999. *Physical Testing of Textiles*. CRC Press.

WANG, J., ZHAO, S., TONG, X., SNYDER, J., AND GUO, B. 2008. Modeling anisotropic surface reflectance with example-based microfacet synthesis. In *ACM SIGGRAPH 2008 papers*, ACM, New York, NY, USA, SIGGRAPH '08, 41:1–41:9.

WEIL, J. 1986. The synthesis of cloth objects. In *Proceedings of the 13th annual conference on Computer graphics and interactive techniques*, ACM, New York, NY, USA, SIGGRAPH '86, 49–54.

WESTIN, S. H., ARVO, J. R., AND TORRANCE, K. E. 1992. Predicting reflectance functions from complex surfaces. *SIGGRAPH Comput. Graph. 26*, 2, 255–264.

XU, Y.-Q., CHEN, Y., LIN, S., ZHONG, H., WU, E., GUO, B., AND SHUM, H.-Y. 2001. Photorealistic rendering of knitwear using the lumislice. In *Proceedings of the 28th annual conference on Computer graphics and interactive techniques*, ACM, New York, NY, USA, SIGGRAPH '01, 391–398.

YASUDA, T., YOKOI, S., TORIWAKI, J.-I., AND INAGAKI, K. 1992. A shading model for cloth objects. *IEEE Comput. Graph. Appl. 12* (November), 15–24.

ZHAO, S., JAKOB, W., MARSCHNER, S., AND BALA, K. 2011. Building volumetric appearance models of fabric using micro ct imaging. *ACM Trans. Graph.* (July).

A   Tangent Distribution Curves

Here we present the tangent distributions that is used for rendering each fabric in this paper. Figure 19 shows the tangent curves of each fabric. The curves are defined by setting the tangent values only at the control points shown in the figure. Table 3 summarizes the tangent offsets of all control points and the length of each segment. The tangent curves are based on the structure of the weaving

pattern. Each flat section on the tangent curve is responsible for a highlight in the BRDF of the fabric.
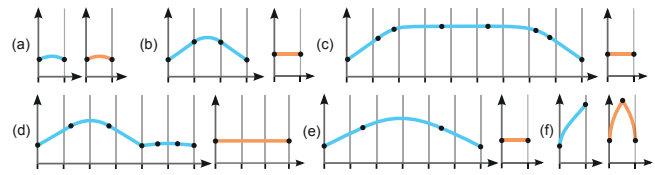

Figure 19: *The tangent curves of all fabrics presented in this paper. The tangent curves are for (a) Linen Plain, (b) Silk Crepe de Chine, (c) front face of Polyester Satin Charmeuse, (d) backface of Polyester Satin Charmeuse, (e) Silk Shot fabric, and (f) Velvet. The numerical values are listed in Table 3.*

Fabric	Thread	α	Tangent Offsets (degrees)	Tangents Lenghts
(a)	Both	0.33	25, 25	1
(b)	Flat	0.75	-35, -35, 35, 35	1, 1, 1
	Twisted	0.25	0, 0	1
(c)	Flat	0.9	-32, -32, -18, 0, 0, 18, 32, 32	1.33, 0.66, 2, 2, 2, 0.66, 1.33
	Twisted	0.1	0, 0	1
(d)	Flat	0.67	-30, -30, 30, 30, -5, -5, 5, 5	1.33, 1.33, 1.33, 0.67, 0.67, 0.67
	Twisted	0.33	0, 0	3
(e)	Dir 1	0.86	-25, -25, 25, 25	1.33, 2.67, 1.33
	Dir 2	0.14	0, 0	1
(f)	Dir 1	0.5	-90, -50	1
	Dir 2	0.5	-90, -55, 55, 90	0.5, 0, 0.5

Table 3: *The list of parameters used to produce the tangent curves for each fabric. The tangent curves are visualized in Figure 19.*